CrossMark

Correlation analysis of heat flux and cone calorimeter test data of commercial flame-retardant ethylene-propylene-diene monomer (EPDM) rubber

Ruiyu Chen[1,2] · Shouxiang Lu[1] · Changhai Li[1] · Yanming Ding[1] · Bosi Zhang[1] ·
Siuming Lo[2]

Abstract The effects of the heat flux on the thermal decomposition of the commercial flame-retardant ethylene-propylene-diene monomer rubber in a cone calorimeter with a piloted ignition were quantitatively investigated. Correlation analysis of the heat flux and various characteristic parameters, including the ignition time, the thermal thickness, the mass loss rate (MLR), the heat release rate (HRR) and the effective heat of combustion, was conducted. It was found that the transformed ignition time $(1/t_{ig})^{0.55}$ and $1/t_{ig}$, the peak and average MLR, the first and second peak HRR, the HRR in the quasi-steady stage and the average HRR all increased linearly with the heat flux. The thermal thickness (δ_P) decreased with the heat flux and was proportional to $\rho/\dot{q}''$. The specimens under the heat fluxes ≤ 35 kW m^{-2} behaved as thermally thin solids, while the thermal decomposition behavior of the specimens under the heat fluxes >35 kW m^{-2} may be characterized employing the thermally thick heating model. The flammability properties including the critical heat flux, the minimum heat flux, the ignition temperature, the heat of gasification and the heat of combustion, which were calculated theoretically based upon the correlations of the ignition time data, the MLR data and the HRR data with the heat flux, were in accordance with the experimental measured values.

Introduction

Increasing attention has been devoted to the metro train fire due to its catastrophic consequence [1–12], such as the fire in the subway of Baku in Azerbaijan in 1995 with 289 people killed and 265 severely injured [11] and the Daegu subway fire in 2003 which resulted in 198 killed and 146 hurt [3]. In China, the fixed flammable materials in the carriage interior of the metro trains mainly comprise the floor coverings and seats, even for some metro trains, inside which the seats are made of non-combustible materials such as stainless steel. In such metro trains, the floor coverings turn out to be the primary fire hazard of the carriage interior. The material under present study is the commercial flame-retardant ethylene-propylene-diene monomer (EPDM) rubber generally used as floor coverings in the metro trains of China. Even though it is flame retarded, it can still be ignited and release large quantities of heat and poisonous gases, especially under high heat fluxes such as the case of severe arson [3], probably involving in the burning of other flammable materials nearby, leading to terrible casualties and property loss. Therefore, study on the fire hazard and the thermal decomposition behavior of the commercial flame-retardant EPDM rubber is fundamental in fire science and also critical in fire safety design of the metro trains.

Cone calorimeter has been widely used to evaluate the fire hazard and investigate the thermal decomposition behavior of materials, such as polyethylene (PE) [13], poly(methyl)methacrylate (PMMA) [14], polystyrene (PS)

✉ Shouxiang Lu
  sxlu@ustc.edu.cn

1 State Key Laboratory of Fire Science, University of Science and Technology of China, Hefei, China

2 Department of Civil and Architectural Engineering, City University of Hong Kong, Hong Kong, China

 Springer

[15–17], poly(vinyl chloride) (PVC) [18], wood [19] and even liquid fuels [20]. However, scarce research on the fire hazard and the thermal decomposition behavior of the commercial flame-retardant EPDM rubber in a cone calorimeter has been reported. Due to the high flammability and smoke yield of the pure EPDM rubber, Song et al. [21], Du et al. [22], Shen et al. [23] and Yen et al. [24] conducted a series of experiments to investigate the effect of the type or proportion of fire retardants such as aluminum hydroxide and magnesium hydroxide on the fire performance of the EPDM rubber employing cone calorimeter. Fire hazard evaluation of the flame-retardant EPDM rubber was performed with the comparison of the ignition time, the peak heat release rate (HRR), the time to peak HRR and the total heat release of the modified flame-retardant EPDM rubber with those of the untreated EPDM rubber merely under one specific heat flux, for example, 35 kW m^{-2}. Thus, the influence of the heat flux on the thermal decomposition behavior of the flame-retardant EPDM rubber was not addressed in their work, which was of considerable significance in reality since the flame-retardant EPDM rubber may present quite different thermal decomposition behaviors under different heat fluxes. In addition, the flammability properties of the flame-retardant EPDM rubber, such as the critical heat flux (CHF), the minimum heat flux, the ignition temperature, the heat of gasification and the heat of combustion, were also not concerned in their studies. But these properties were demonstrated fundamentally to have a notable impact on the fire hazard and the thermal decomposition process of materials [25–27] and should be determined to deeply understand the potential influencing factors in essence for the fire hazard and the thermal decomposition behavior of the flame-retardant EPDM rubber. Furthermore, these flammability properties were the basis for the numerical simulation of the thermal decomposition behavior of the commercial flame-retardant EPDM rubber as well as the metro train fires, which can provide guidance for the full-scale metro train fire experiments [11] and fire safety design of the metro trains [10]. In sum, much work needs to be carried out to quantitatively analyze the fire hazard and the thermal decomposition behavior of the commercial flame-retardant EPDM rubber in essence, considering the effects of the heat flux on the thermal decomposition of the commercial flame-retardant EPDM rubber.

The present study quantitatively examined the characteristic parameters for the thermal decomposition of the commercial flame-retardant EPDM rubber, including the ignition time, the thermal thickness, the mass loss rate (MLR), the HRR and the effective heat of combustion (EHC) in a cone calorimeter under piloted ignition and a widespread range of heat fluxes. Correlation analysis of the heat flux and the characteristic parameters was conducted.

The flammability properties including the CHF, the minimum heat flux, the ignition temperature, the heat of gasification and the heat of combustion of the commercial flame-retardant EPDM rubber were theoretically deduced based upon the correlation analysis and verified.

Experimental

Materials

The basic properties of the commercial flame-retardant EPDM rubber are shown in Table 1. The density ρ and the limiting oxygen index (LOI) were provided by the manufacturer. The ignition temperature and the heat of combustion were measured according to ISO 871 [28] and ISO 1716 [29], respectively. A Hot Disk TPS 2500s was employed to obtain the specific heat c, the thermal conductivity λ and the thermal diffusivity α. Table 2 illustrates the compositions and the corresponding mass fraction of the commercial flame-retardant EPDM rubber.

Measurement

The tests were carried out employing a cone calorimeter conforming to ISO 5660-1 standard [30] with a digital electronic balance (UX6200H) whose accuracy was 0.01 g. The mass of the specimens with the dimensions of 99 ± 1 mm (length), 99 ± 1 mm (width) and 3 mm (thickness) was 52 ± 1.6 g. The specimens, whose edges and rear surface were wrapped with aluminum foil, were horizontally located 25 mm from the cone heater. Ceramic fiber blanket was placed under the specimens for heat insulation. Ten heat flux levels were used from 20 to 65 kW m^{-2} with the interval of 5 kW m^{-2}. The specimens were found to intumesce considerably and even contact the spark igniter under almost all the applied heat fluxes in the preliminary experiments without wire grid, leading to poor accuracy and repeatability of the measurements such as the

Table 1 Basic properties of the commercial flame-retardant EPDM rubber

Category	Value
Density ρ/kg m^{-3}	1500
Specific heat c/J kg^{-1} K^{-1}	1020
Thermal conductivity λ/W m^{-1} K^{-1}	0.102
Thermal diffusivity α/m^2 s^{-1}	6.67×10^{-8}
Ignition temperature/K	703
Heat of combustion/MJ kg^{-1}	14.62
LOI/%	35.7

Table 2 Compositions and corresponding mass fraction of the commercial flame-retardant EPDM rubber

Category	Mass fraction/ %
Pure EPDM rubber	27
Microencapsulated red phosphorus	1.5
Decabromodiphenyl ethane	6
Magnesium hydroxide	10
Aluminum hydroxide	20
Antimonous oxide	4
Zinc borate	6
Fire retardant dedicated for polyolefin (HT-101)	1.8
Zinc oxide	0.6
Stearic acid	0.2
Ozone-resistant antiager (MB)	0.8
Oxygen-resistant antiager (SP)	1.2
Precipitated silica	4
Pulvis talci	6
Titanium dioxide	5
Dispersing agent (WB-16)	0.5
Surfactant (PEG 4000)	1.5
Microcrystalline wax	0.5
Antioxidant (B225)	0.4
Yellowing-resistant accelerator (AG 201)	0.4
Vulcanization accelerator (TMTD, TiBTM)	1.8
Insoluble sulfur	0.8

ignition time, the MLR and the HRR. Therefore, to prevent the specimen from intumescing as well as to reduce the influence of the wire grid on the measurements, an appropriate wire grid made of 2-mm stainless steel rod with all intersections welded was adopted according to Refs. [30–32], as illustrated in Fig. 1. Tests were conducted with
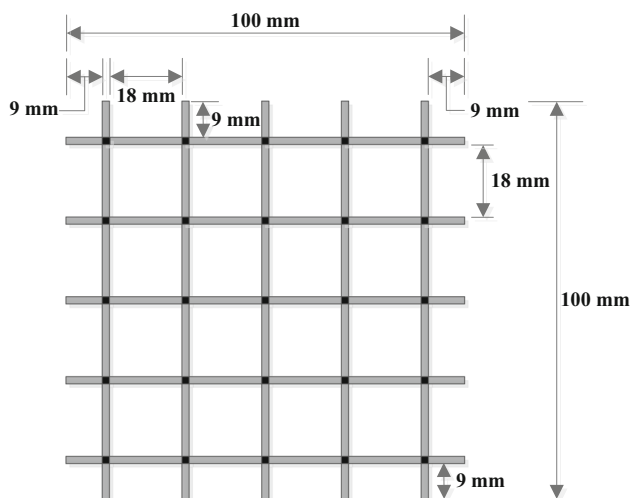
Fig. 1 Schematic of wire grid

a piloted ignition in air with ambient temperature of 298 ± 2 K and relative humidity of 50 ± 5 %. Calibration of the cone calorimeter was conducted before each test according to Ref. [30]. Termination of the experiment was performed manually if no ignition was observed for 32 min after the initiation of the experiment [33]. Each test was repeated once, and the average value of the two test results was used for analysis.

Results and discussion

Ignition time

Ignition time is one of the critical parameters to characterize the fire hazard and the thermal decomposition behavior of materials [14, 25, 26, 34]. Specimen with high ignition time possesses low fire hazard and high thermal resistance. Correlation of the ignition time with the heat flux can be employed to determine whether the specimen behaves as thermally thick materials in which heterogeneous temperature profile occurs or thermally thin materials where temperature distributes approximately homogeneously when exposed to external heat [35]. Furthermore, correlation of the ignition time with the heat flux may be used to obtain the flammability properties of materials, such as the CHF and the ignition temperature.

A summary of ignition time data under a series of heat fluxes is presented in Table 3. It is observed in Table 3 that the ignition time decreased with an increase in the heat flux. The ignition time under low heat fluxes was several times as large as that under high heat fluxes.

Numerous correlations, which are based upon the ignition time data, the heat flux and the thermophysical properties of the materials, were proposed to analyze the thermal decomposition of the materials [19, 34]. The opinion of Janssens [36, 37] is considered to be the best means for the analysis of the thermal decomposition of

Table 3 Summary of ignition time data

Heat flux/kW m^{-2}	Ignition time/s
25	488
30	202
35	158
40	110
45	77
50	58
55	42
60	40
65	38

thermally thick solids and can be also employed to identify whether materials are thermally thick or thermally thin materials [4, 34].

According to the research of Janssens [36, 37], the transformed ignition time $(1/t_{ig})^n$ was firstly correlated with the heat flux employing different values of n (t_{ig} denotes the ignition time, n is a coefficient, $n = 0.55$ and 1 correspond to the cases of thermally thick and thermally thin solids, respectively). Then, the least-squares method was adopted to obtain the correlation coefficient R^2. The value of n with the higher R^2 was finally adopted. However, as illustrated in Fig. 2, the value of R^2 corresponding to the case of $n = 0.55$ (0.9752) is merely slightly higher than that corresponding to the case of $n = 1$ (0.9686). Therefore, it may be not convincing if the specimens were simply concluded to be thermally thick solids under all the heat fluxes in the present study by following the opinions of Janssens. The correlations of the transformed ignition time with the heat flux for the cases of $n = 0.55$ and 1 are presented as follows:

$$(1/t_{ig})^{0.55} = 0.0027 \dot{q}_e'' - 0.0297 \tag{1}$$

$$1/t_{ig} = 6.6775 \times 10^{-4} \dot{q}_e'' - 0.01585 \tag{2}$$

where t_{ig} denotes the ignition time (s). $\dot{q}_e''$ denotes the heat flux (kW m^{-2}).

It was widely reported that the x-axis intercept of the fitting line in Fig. 2 represented the theoretical CHF $\dot{q}_{cr}''$ [13, 14, 25–27, 34, 36, 37], which was calculated to be 11 kW m^{-2} ($n = 0.55$) and 23.7362 kW m^{-2} ($n = 1$). Difference between the theoretical CHF $\dot{q}_{cr}''$ and the experimental minimum heat flux $\dot{q}_{min}''$ was presented [34, 37]. $\dot{q}_{cr}''$ is generally determined from the curve fitting of the ignition time data with the applied heat fluxes. However, $\dot{q}_{min}''$ denotes the heat flux which was just sufficient to heat the material surface to the ignition temperature for very

long exposure times (theoretically ∞) [14, 38–40]. In fact, it is difficult to determine the accurate value of the minimum heat flux of the materials. However, for engineering purpose, the minimum heat flux of the specimen can be considered as the average value of the lowest heat flux at which ignition of the specimen was found and the highest heat flux at which no ignition occurred to the specimen for 32 min [20, 33, 34, 36, 37, 41] for convenience. Thus, $\dot{q}_{min}''$ was deduced to be 22.5 kW m^{-2} in the present study since ignition did not occur to the specimen after the specimen was exposed under the heat flux of 20 kW m^{-2} for 32 min, while ignition of the specimen was found under the heat flux of 25 kW m^{-2} within 32 min. Based upon a series of experimental results, $\dot{q}_{min}''$ was found to be 2.4 times as large as $\dot{q}_{cr}''$ [34]:

$$\dot{q}_{min}'' = 2.4\dot{q}_{cr}'' \tag{3}$$

Thus, $\dot{q}_{min}''$ can be theoretically calculated to be 26.4 and 56.9669 kW m^{-2} from $\dot{q}_{cr}''$ in the cases of $n = 0.55$ and 1, respectively, in the present study. The theoretical calculated value of $\dot{q}_{min}''$ in the case of $n = 0.55$ was almost consistent with the experimental measured value of $\dot{q}_{min}''$ (22.5 kW m^{-2}) on account of the uncertainties of the measurement and calculation method. However, the theoretical calculated value of $\dot{q}_{min}''$ in the case of $n = 1$ was much larger than the experimental measured value of $\dot{q}_{min}''$ (22.5 kW m^{-2}), which may indicate that the thermally thin heating model was not suitable for the characterization of the thermal decomposition behaviors of the specimens under all the heat fluxes in the present study.

It was highlighted that the ignition temperature of the specimen can be more accurately obtained from $\dot{q}_{min}''$ rather than $\dot{q}_{cr}''$ [34], as shown in Eq. (4).

$$\varepsilon\dot{q}_{min}'' = h_c(T_{ig} - T_\infty) + \varepsilon\sigma(T_{ig}^4 - T_\infty^4) \tag{4}$$
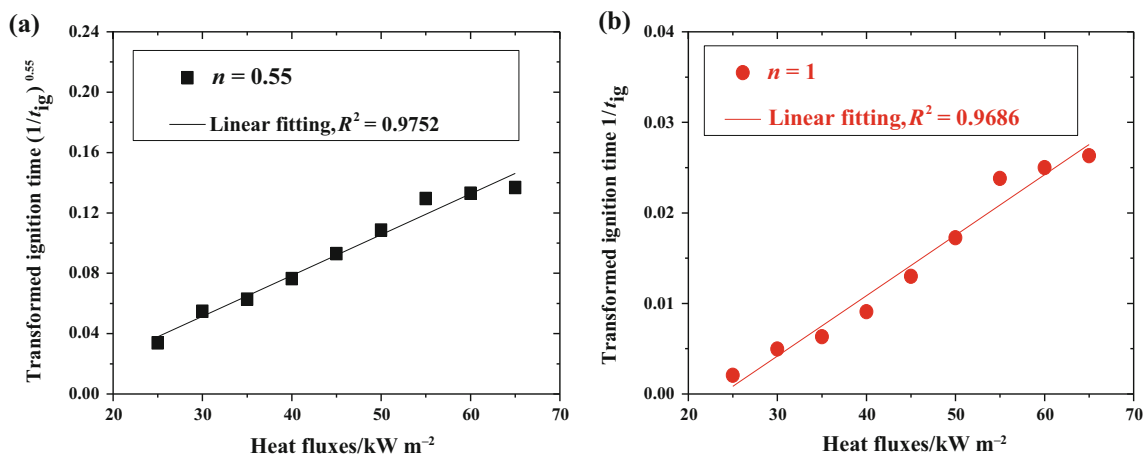

Fig. 2 Transformed ignition time $(1/t_{ig})^n$ as a function of heat flux: **a** $n = 0.55$; **b** $n = 1$

where h_c denotes the convective heat transfer coefficient and was taken as 0.0135 kW m^{-2} K^{-1} [34] in the present study. ε represents the surface emissivity of the specimen at ignition and was taken as 0.88 [4, 34] in the present study. σ is the Stefan–Boltzmann constant (5.67×10^{-11} kW m^{-2} K^{-4}). T_{ig} and T_∞ denote the ignition temperature of the specimen and the ambient temperature (K), respectively.

A MATLAB program was developed to obtain the iterative solution of Eq. (4). The ignition temperature of the specimen was calculated to be 732.08 K, the accuracy of which can be acceptable in comparison with the experimental measured value of the ignition temperature of the specimen (703 K) for engineering purpose, as demonstrated in Table 1.

Thermal thickness

The thermal thickness of a material can be considered as the thermal penetration depth of the material at ignition, which is defined as the thickness of the specimen which has been heated to a certain temperature [15, 19, 34]. Thus, the thermal penetration depth of the material at ignition can be also employed to distinguish whether the specimen behaves as thermally thick or thermally thin materials when exposed to external heat. The specimen can be regarded as thermally thick material if the thermal penetration depth of the specimen at ignition is less than the physical thickness of the specimen, meaning that the external heat could not reach the bottom of the specimen at ignition and, thus, heterogeneous temperature profile occurs inside the specimen. On the contrary, the specimen is considered to be thermally thin material if the thermal penetration depth of the specimen at ignition is larger than the physical thickness of the specimen. The thermal penetration depth of the specimen at ignition, namely the thermal thickness, can be calculated according to the following equation [34]:

$$\delta_P = A\sqrt{\frac{\lambda t_{ig}}{\rho_c}} \tag{5}$$

where δ_P denotes the thermal thickness of the specimen (m). A is a constant and taken as 1 in the present study based upon the work of Mikkola and Wichman [42].

Babrauskas [34] pointed out that for wood products, the thermal thickness of the specimen may be also estimated by:

$$\delta_P = \frac{0.6\rho}{\dot{q}_e''} \tag{6}$$

Taking Eqs. (5) and (6) into comparison, it can be concluded that it is easier to obtain the thermal thickness of the specimen employing Eq. (6) than Eq. (5), since merely the density of the specimen and the applied heat flux are required and both of the two parameters are easy to get. Even though Eq. (6) was proposed based upon the results of wood products, similar simple and convenient correlation to Eq. (6) may be developed to acquire the thermal thickness of the specimen for the commercial flame-retardant EPDM rubber under present study. Thus, the results from Eqs. (5) and (6) were correlated, as shown in Fig. 3. The vertical ordinate and the abscissa in Fig. 3 denote the results calculated from Eqs. (5) and (6), respectively. It is illustrated in Fig. 3 that the thermal thickness of the commercial flame-retardant EPDM rubber δ_P is proportional to $\rho/\dot{q}''$ and high correlation coefficient R^2 is demonstrated. Therefore, the thermal thickness of the commercial flame-retardant EPDM rubber can be estimated by:

$$\delta_P = 0.0772\left(\frac{\rho}{\dot{q}_e''}\right) \tag{7}$$

The correlation shown in Eq. (7) presents similar form to those proposed by the previous researchers [34], who suggested the correlation of $\delta_P = C\rho/\dot{q}''$. However, the values of C are different. The values of C were 0.6 and 0.14 for wood products [34] and various non-flame-retardant polymers [43], respectively, but the value of C in the present study was merely 0.0772.

As we can see from Fig. 3, the thermal thickness of the specimen increased with a decrease in the heat flux. The thermal thickness of the specimens under the heat fluxes greater than 35 kW m^{-2} was less than 3 mm (the physical thickness of the specimen), which suggested that the specimens under the heat fluxes greater than 35 kW m^{-2} were prone to be thermally thick solids under present study. However, the thermal thickness of the specimens was
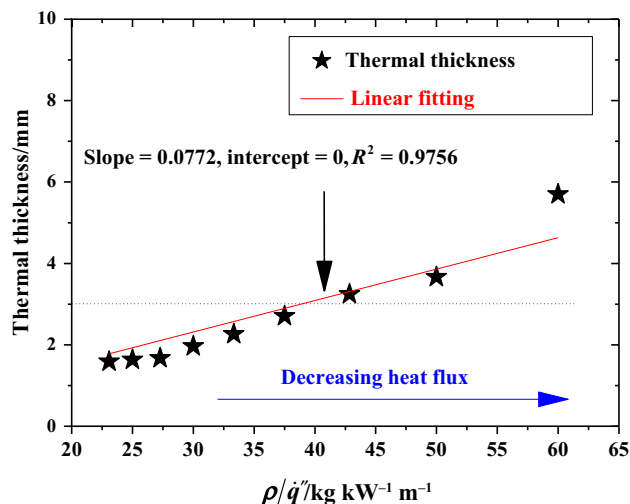

Fig. 3 Correlation between thermal thickness, density and heat flux

larger than 3 mm under the heat fluxes ≤ 35 kW m^{-2}, probably indicating that the thermal decomposition behavior of the specimens under the heat fluxes ≤ 35 kW m^{-2} could be characterized by the thermally thin heating model. Such phenomenon may explain why the difference of the value of R^2 corresponding to the cases of $n = 0.55$ and 1 was small, as illustrated in Fig. 2.

Mass loss rate

MLR is defined as the mass loss rate of solid or liquid fuel vaporized and burned [44, 45]. It can be adopted to characterize the thermal decomposition rate of the specimen and thus evaluate the fire hazard of the materials. The peak MLR, the time to peak MLR and the average MLR are presented in Table 4.

As presented in Table 4, the peak and average MLR both increased with the heat flux. The time to attain the peak MLR was shortened as the heat flux increased. As illustrated in Fig. 4, the transient MLR can be estimated as [46]:

$$\dot{m}'' = \frac{1}{L}\left(\dot{q}_e'' + \dot{q}_{f,c}'' + \dot{q}_{f,r}'' - \dot{q}_{cond}'' - \sigma(T_V^4 - T_\infty^4)\right) \quad (8)$$

where $\dot{m}''$ denotes the transient MLR of the specimen (g s^{-1} m^{-2}). L represents the heat of gasification of the specimen (kJ g^{-1}). $\dot{q}_{f,c}''$ and $\dot{q}_{f,r}''$ are the convective and radiative heat flux from the flame (kW m^{-2}), respectively. $\dot{q}_{cond}''$ denotes the thermal conduction loss from the specimen (kW m^{-2}). $\sigma(T_V^4 - T_\infty^4)$ denotes the surface re-radiation heat loss of the specimen (kW m^{-2}). T_V is the vaporization temperature of the specimen (K).

For engineering purpose, according to the Refs. [25, 39, 46–51], for a given material and specimen size, the convective heat flux from the flame $\dot{q}_{f,c}''$ and the radiative heat flux from the flame $\dot{q}_{f,r}''$ can be both considered as approximately constant in the cases of steady (or quasi-steady) burning or at the moment of the peak MLRs.
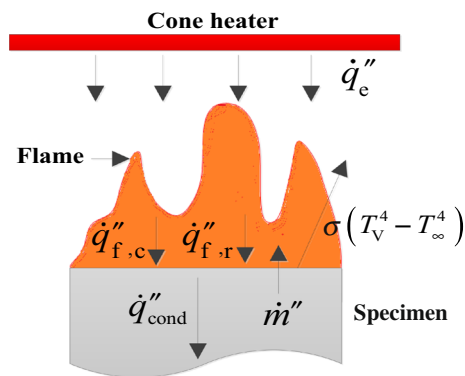

Fig. 4 Heat transfer schematic of the thermal decomposition of the specimen

In addition, the thermal conduction loss from the specimen $\dot{q}_{cond}''$ can be accounted for in the heat of gasification of the specimen L under steady (or quasi-steady) burning or at the moment of the peak MLRs. Furthermore, the vaporization temperature of the specimen T_V can be approximated as being equal to the ignition temperature of the specimen, which is a constant for specific materials and fixed specimen size. Thus, all the terms except $\dot{q}_e''$ in the right side of Eq. (8) can be taken as constants under steady (or quasi-steady) burning or at the moment of the peak MLRs, as illustrated in Eq. (9). Thus, the peak MLR and the average MLR may be linearly correlated with the applied heat flux $\dot{q}_e''$.

$$\dot{m}'' = \frac{1}{L}\dot{q}_e'' + C \quad (9)$$

where C is a constant.

Figure 5 shows the variations of the peak and average MLR versus heat flux. As demonstrated in Fig. 5, excellent linear fitting of the peak MLR with the heat flux was

Table 4 Summary of MLR data

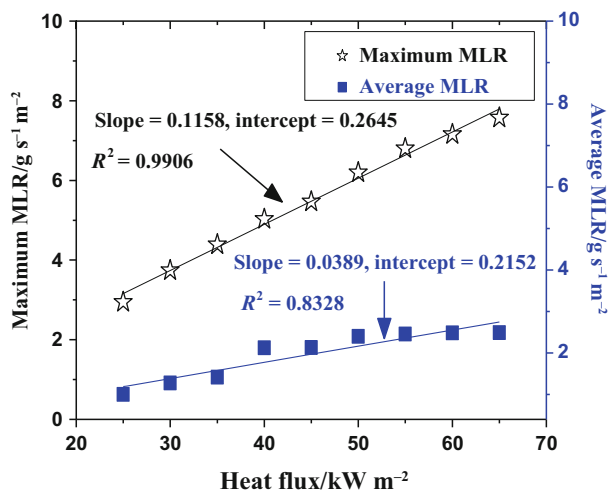| Heat flux/kW m^{-2}	Peak MLR/g s^{-1} m^{-2}	Time to peak MLR/s	Average MLR/g s^{-1} m^{-2}
25	2.9448	564	1.0009
30	3.7381	287	1.2789
35	4.3911	201	1.4195
40	5.0283	155	2.1244
45	5.4651	144	2.1283
50	6.1974	123	2.4015
55	6.7972	120	2.4561
60	7.1571	109	2.4862
65	7.5724	103	2.4921

Fig. 5 Peak and average MLR versus heat flux

obtained, but the linearity of the correlation of the average MLR with the heat flux was not very good. The corresponding correlations are presented as Eqs. (10) and (11).

$$\dot{m}_P'' = 0.1158\dot{q}_e'' + 0.2645 \tag{10}$$

$$\bar{m}'' = 0.0389\dot{q}_e'' + 0.2152 \tag{11}$$

where $\dot{m}_P''$ and $\bar{m}''$ denote the peak MLR and the average MLR (g s^{-1} m^{-2}), respectively.

As illustrated in Eq. (9) and Fig. 5, the heat of gasification of the specimen L refers to the reciprocal of the slope of the fitting line, and it was calculated to be 8.6356 MJ kg^{-1} (labeled as "L_1") and 25.7069 MJ kg^{-1} (labeled as "L_2") from the fitting line of the peak and average MLR with the heat flux, respectively. L_2 was much larger than L_1. It may be due to that the whole thermal decomposition process of the commercial flame-retardant EPDM rubber could not be considered as steady or quasi-steady burning [52] and the average MLR cannot be considered to strictly follow linear relationship with the heat flux as shown in Eq. (9), leading to not so convincing correlation of the average MLR with the heat flux (the corresponding correlation coefficient R^2 was only 0.8328) and the calculated heat of gasification. Therefore, the heat of gasification obtained from the correlation of the peak MLR with the heat flux L_1 was adopted in the present study.

Heat release rate

HRR represents the rate of thermal energy released from the combustion of the materials and is considered as the single most important variable in fire hazard evaluation [13, 53]. The HRR was calculated adopting the oxygen consumption calorimetry technique based upon the ISO

5660-1 standard [13, 14, 30, 34, 53–55] by measuring the concentration of the generated gaseous compounds (O_2, CO_2, CO, etc.) from the combustion of the specimens. Figure 6 depicts the variations in HRR versus experimental time. More detailed information about the HRR is illustrated in Table 5.

As shown in Fig. 6 and Table 5, two peak HRRs and a quasi-steady stage between the first peak HRR and the second peak HRR occurred in the cases of the heat fluxes greater than 35 kW m^{-2}, while only one peak HRR and no quasi-steady stage were found under the heat fluxes below or equal to 35 kW m^{-2}. The first peak HRR, the second peak HRR and the HRR in the quasi-steady stage all increased with the heat flux. The average HRR generally rose as the heat flux increased. It should be noted that the average HRR was obtained by integrating an HRR curve from the time of ignition to the moment of final drop of HRR below 20 kW m^{-2} and subsequent division of the integral value by the length of the time period used in the integration. This was to cut off part of the curves dominated by signal noise, which was notably higher in amplitude at the end of test than at the outset [43, 56]. Besides employing the oxygen consumption calorimetry technique to obtain the transient HRR as discussed above, the transient HRR can be also acquired through the transient MLR and the theoretical heat of combustion of the specimen:

$$\begin{aligned}\dot{q}'' &= \dot{m}''\Delta H_c^T \\ &= \frac{\Delta H_c^T}{L}\left(\dot{q}_e'' + \dot{q}_{f,c}'' + \dot{q}_{f,r}'' - \dot{q}_{cond}'' - \sigma\left(T_V^4 - T_\infty^4\right)\right)\end{aligned} \tag{12}$$

where $\dot{q}''$ represents the transient HRR (kW m^{-2}). ΔH_c^T denotes the theoretical heat of combustion of the specimen (kJ g^{-1}), representing the nominal heat released from the complete combustion of per unit mass of materials, and it was measured to be 14.62 MJ kg^{-1} using an oxygen bomb calorimeter [29], as shown in Table 1.

As demonstrated in "Mass loss rate" section, the peak and average MLR can be linearly correlated with the heat flux. According to Eq. (12), the HRR is proportional to the MLR with constant theoretical heat of combustion ΔH_c^T for a specific material. Thus, the peak HRR, the average HRR and the HRR in the quasi-steady stage may follow the similar behavior to the correlation of the peak and average MLR with the heat flux, as shown in Eq. (13).

$$\dot{q}'' = \dot{m}''\Delta H_c^T = \frac{\Delta H_c^T}{L}\dot{q}_e'' + C_1 \tag{13}$$

where C_1 is a constant. As presented in Eq. (13), the theoretical heat of combustion ΔH_c^T can be obtained from the slope of the linear fitting line of the HRR under the steady (or quasi-steady) burning or the peak HRR with the heat
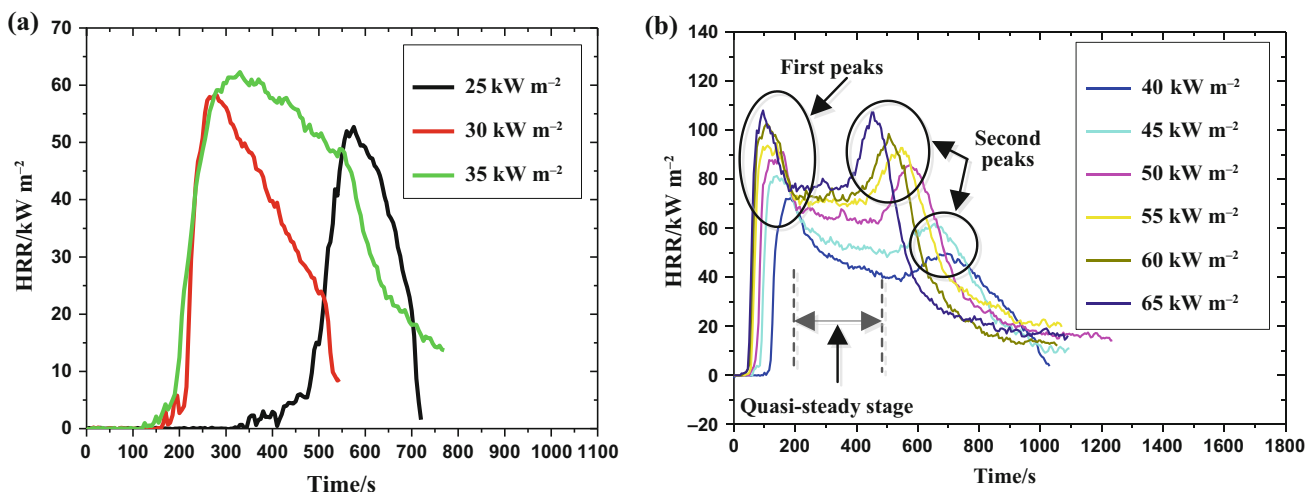
Fig. 6 HRR versus experimental time

Table 5 Summary of HRR data

| Heat flux/ kW m^{-2}	First peak HRR/ kW m^{-2}	Time to first peak HRR/s	HRR in quasi-steady stage/kW m^{-2}	Second peak HRR/ kW m^{-2}	Time to second peak HRR/s	Average HRR/ kW m^{-2}
25	52.7086	575	–	–	–	37.7471
30	58.2587	280	–	–	–	39.6837
35	62.3055	330	–	–	–	43.4254
40	72.2950	185	43.7951	49.6726	695	44.3186
45	81.3387	140	53.0545	61.7961	654	52.3767
50	91.0299	160	64.9186	85.9779	575	57.0774
55	94.7407	140	70.7142	92.7384	545	55.9546
60	102.3761	106	72.8125	98.4342	505	66.4195
65	107.9378	95	76.7737	107.2698	455	62.4399
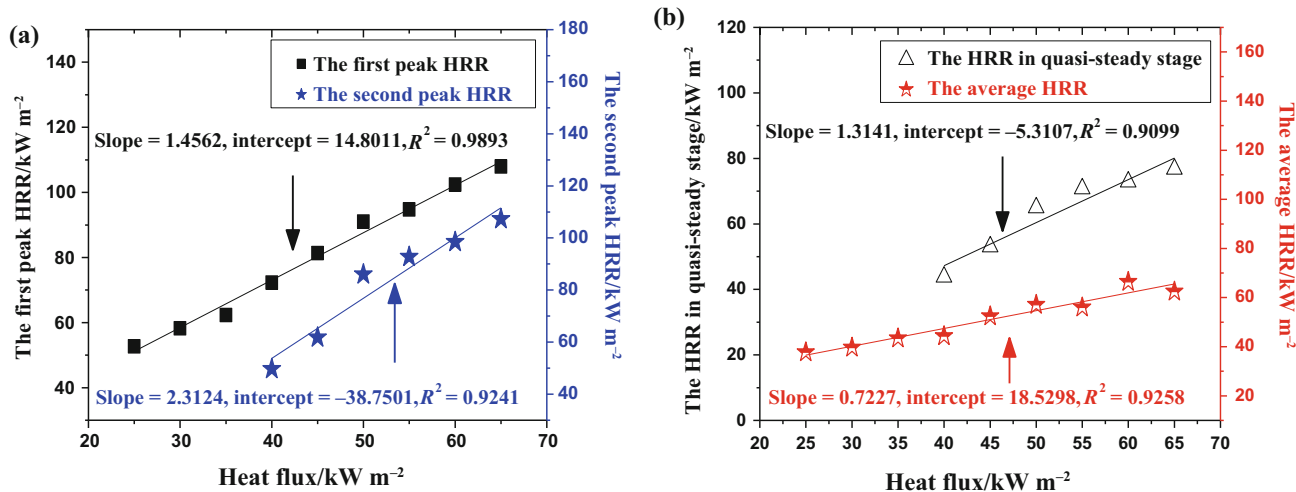
Fig. 7 The first and second peak HRR, the HRR in the quasi-steady stage and the average HRR versus heat flux

flux after the heat of gasification of the specimen L was acquired from the MLR data.

The first and second peak HRR, the average HRR and the HRR in the quasi-steady stage as a function of the heat flux are thus shown in Fig. 7. As we can see from Fig. 7, the first and second peak HRR, the average HRR and the HRR in the quasi-steady stage can be correlated with the heat flux as:

$$\dot{q}''_{\text{fp}} = 1.4562\dot{q}''_{\text{e}} + 14.8011 \tag{14}$$

$$\dot{q}''_{\text{sp}} = 2.3124\dot{q}''_{\text{e}} - 38.7501 \tag{15}$$

$$\bar{\dot{q}}'' = 0.7227\dot{q}''_{\text{e}} + 18.5298 \tag{16}$$

$$\dot{q}''_{\text{qs}} = 1.3141\dot{q}''_{\text{e}} - 5.3107 \tag{17}$$

where $\dot{q}''_{\text{fp}}$, $\dot{q}''_{\text{sp}}$, $\bar{\dot{q}}''$, $\dot{q}''_{\text{qs}}$ denote the first peak HRR, the second peak HRR, the average HRR and the HRR in the quasi-steady stage (kW m^{-2}), respectively.

Based upon Eqs. (13)–(17) and the calculated theoretical heat of gasification from the MLR data, as discussed in "Mass loss rate" section, the theoretical heat of combustion $\Delta H_{\text{c}}^{\text{T}}$ can be deduced to be 12.5756 MJ kg^{-1} (from the first peak HRR data), 19.9689 MJ kg^{-1} (from the second peak HRR data), 6.2405 MJ kg^{-1} (from the average HRR data) and 11.3478 MJ kg^{-1} (from the HRR data in the quasi-steady stage). As noted in "Mass loss rate" section and Fig. 6, the whole decomposition process of the specimen cannot be considered as a steady or quasi-steady stage. Thus, it may be more reasonable to select the peak HRR data to calculate the theoretical heat of combustion instead of the average HRR data. Furthermore, since the correlation coefficient R^2 of the fitting of the first peak HRR with the heat flux is the highest, as depicted in Fig. 7, it contains all the first peak HRR data from all the cases, while the second peak HRR and the HRR in the quasi-steady stage merely occurred in the cases of the heat fluxes greater than 35 kW m^{-2}, and thus, the theoretical heat of combustion obtained through the first peak HRR data may be considered to best reflect the general characteristic for the thermal decomposition of the commercial flame-retardant EPDM rubber under all the heat fluxes. Therefore, the theoretical heat of combustion was taken as 12.5756 MJ kg^{-1} in the present study, which was almost in accordance with that measured using an oxygen bomb calorimeter (14.62 MJ kg^{-1}). The difference may be due to the incomplete combustion of the specimen and the uncertainty of the measurement and calculation method. This validated that the first peak HRR data can be adopted to obtain the theoretical heat of combustion of the commercial flame-retardant EPDM rubber under present study. Since the considerably accurate theoretical heat of combustion was obtained based upon the theoretical calculated heat of gasification L from the peak MLR data, this may verify that

the accuracy of the theoretical calculated heat of gasification L from the peak MLR data could be acceptable.

Effective heat of combustion

In fact, the combustion of materials cannot be strictly complete. It is greatly influenced by the amount of the oxygen in the combustion region. The incomplete combustion of the materials will occur due to the lack of sufficient oxygen in the combustion region, leading to lower heat of combustion of the materials actually in comparison with the theoretical heat of combustion of the materials. The EHC denotes the actual heat released from the burning of per unit mass of materials. It can be used to characterize the capability of the materials to release heat in reality. In the present study, the EHC varied with time and heat flux. It can be calculated from the transient HRR and MLR as follows:

$$\Delta H_{\text{c}}^{\text{E}} = \frac{\dot{q}''}{\dot{m}''} \tag{18}$$

where $\Delta H_{\text{c}}^{\text{E}}$ denotes the transient EHC (kJ g^{-1}).

The variations in EHC versus experimental time are presented in Fig. 8. Note that the moment of the end of the EHC curves corresponded to the moment of the final drop of HRR below 20 kW m^{-2}. This was to decrease the influence from the signal noise resulted by the measurement system, as discussed in "Heat release rate" section. Table 6 illustrates the first peak EHC, the second peak EHC and the average EHC. As can be observed from Fig. 8 and Table 6, in accordance with the HRR curves and obtained theoretical heat of combustion, there were two peak EHCs in the cases of the heat fluxes larger than 35 kW m^{-2}, while only one peak EHC appeared in the cases of 25, 30 and 35 kW m^{-2}. Moreover, the second peak EHCs were much larger than the corresponding first peak EHCs for the cases of the heat fluxes greater than 35 kW m^{-2}. This was likely attributed to that [52]: At the moment of the second peak EHCs under high heat fluxes, the effectiveness of fire retardants to the EPDM rubber may be lost. Thus, the char layer that generated above the remained virgin specimen cracked. The remained virgin specimen was more uniformly decomposed and released flammable gases of higher concentration. As a consequence, the specimen burned more fiercely, which was consistent with the observed flame behavior. Therefore, more effective combustion of the specimen occurred, resulting in higher EHC values.

As shown in Table 6, the average EHC (16.4341 MJ kg^{-1}) was almost in accordance with the theoretical heat of combustion obtained from the first peak HRR data (12.5756 MJ kg^{-1}), as discussed in "Heat release rate" section. In addition, the average EHC (16.4341 MJ kg^{-1})

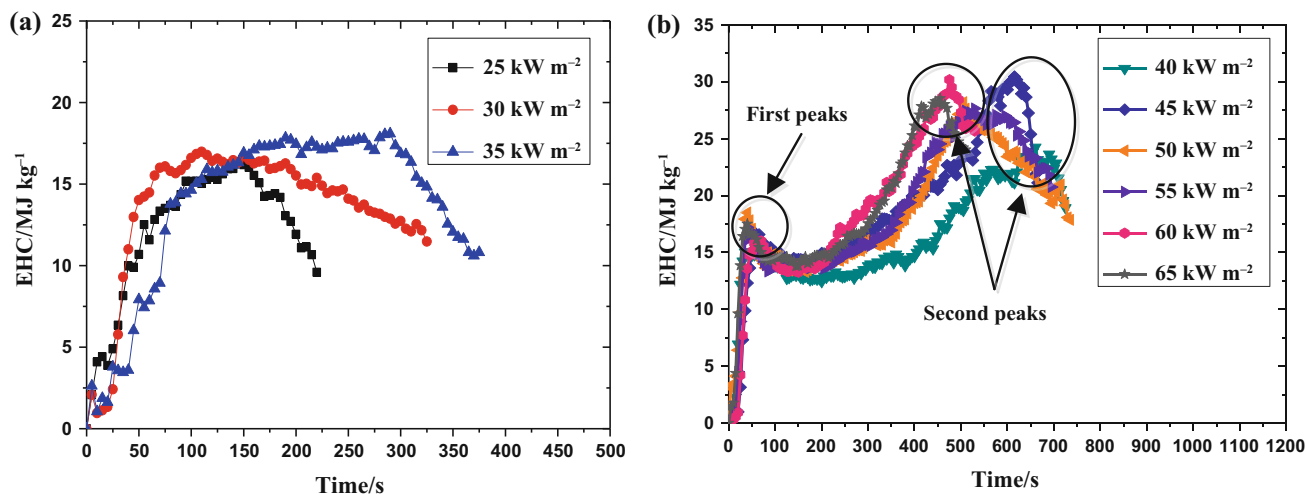**Fig. 8** EHC versus experimental time

Table 6 Summary of EHC data

Heat flux/kW m^{-2}	The first peak EHC/MJ kg^{-1}	The second peak EHC/MJ kg^{-1}	The average EHC/MJ kg^{-1}
25	16.3498	–	12.0068
30	16.9764	–	13.4023
35	18.0892	–	13.6002
40	15.0631	24.2438	16.2194
45	16.7659	30.4625	18.6581
50	18.5085	28.1889	18.4328
55	17.2003	27.6495	18.8818
60	16.0141	30.1908	18.3965
65	17.5091	28.5391	18.3086
Average value	16.9418	28.2124	16.4341

was also nearly consistent with the theoretical heat of combustion measured by an oxygen bomb calorimeter (14.62 MJ kg^{-1}), as illustrated in Table 1. Furthermore, the difference between the average value of the first peak EHCs (16.9418 MJ kg^{-1}) and the theoretical heat of combustion acquired from the first peak HRR data (12.5756 MJ kg^{-1}) may be acceptable for engineering application. It was the same to the case of the average value of the second peak EHCs (28.2124 MJ kg^{-1}) and the theoretical heat of combustion acquired from the second peak HRR data (19.9689 MJ kg^{-1}). However, the average EHC (16.4341 MJ kg^{-1}) was much larger than the theoretical heat of combustion deduced from the average HRR data (6.2405 MJ kg^{-1}). This may further indicate that the whole thermal decomposition process of the specimens under present study cannot be considered as a steady stage. The average HRR data may not be used to estimate the theoretical heat of combustion under present study. Instead, the peak HRR data may be employed to obtain the relatively

accurate theoretical heat of combustion for the thermal decomposition of the commercial flame-retardant EPDM rubber.

Conclusions

The characteristic parameters for the thermal decomposition of the commercial flame-retardant EPDM rubber, including the ignition time, the thermal thickness, the MLR, the HRR and the EHC, were quantitatively investigated employing cone calorimeter under piloted ignition and a series of heat fluxes experimentally. Correlation analysis of the heat flux and the characteristic parameters was performed. Based upon the correlation and theoretical analyses, the flammability properties including the CHF, the minimum heat flux, the ignition temperature, the heat of gasification and the heat of combustion were deduced. The main conclusions are addressed as follows:

1. Both of the transformed ignition time $(1/t_{ig})^{0.55}$ and $1/t_{ig}$ followed a linear relation to the heat flux, allowing calculation of the minimum heat flux and the ignition temperature. The calculated minimum heat flux based upon the correlation of the transformed ignition time $(1/t_{ig})^{0.55}$ with the heat flux was found to be almost consistent with the experimental measured value. The calculated ignition temperature based upon the minimum heat flux was also nearly in accordance with the experimental measured ignition temperature.

The thermal thickness of the specimen δ_P was demonstrated to be proportional to the ratio of the density of the specimen and the applied heat flux $\rho/\dot{q}''$. In addition, the thermal thickness of the specimens under the heat fluxes >35 kW m^{-2} was less than 3 mm, suggesting that the specimens under the heat fluxes >35 kW m^{-2} presented the characteristic of the thermally thick solids. However, the thermal thickness of the specimens under the heat fluxes ≤35 kW m^{-2} was larger than 3 mm, indicating that the thermal decomposition behavior of the specimens under heat fluxes ≤35 kW m^{-2} may be characterized using the thermally thin heating model.

2. Linear correlations of the peak and average MLR with the heat flux were obtained. The heat of gasification of the specimen was calculated based upon the correlations and theoretical analysis. It was found that the heat of gasification of the specimen acquired from the peak MLR data was more reliable than that through the average MLR data.

3. Two peak HRRs and a quasi-steady stage between the first peak HRR and the second peak HRR were noted in the HRR evolution under the heat fluxes greater than 35 kW m^{-2}. The first and second peak HRR, the HRR in the quasi-steady stage and the average HRR all increased linearly with the heat flux, and the corresponding correlations were acquired. The theoretical heat of combustion of the specimen was obtained through the correlations with theoretical analysis and compared with the experimental measured value. The theoretical heat of combustion of the specimen calculated from the first peak HRR data was demonstrated to best reflect the general characteristic for the thermal decomposition of the specimen.

4. In the cases of heat fluxes larger than 35 kW m^{-2}, two peak EHCs occurred in the EHC curves, and the second peak EHC was much larger than the first peak EHC. The average value of the first peak EHC and the average EHC were almost in accordance with the theoretical calculated heat of combustion from the first peak HRR data and the experimental measured heat of combustion.

The present study is part of the research on fire dynamics of the urban underground space under complex boundaries. The conclusion obtained under current study may provide practical guidance to fire safety design of the urban underground space.

References

1. Duggan G. Usage of ISO 5660 data in UK railway standards and fire safety cases. In: A one-day conference on fire hazards, testing, Materials and products. Shrewsbury: Rapra Technology Ltd; 1997. p. 1–8.
2. Haack A. Fire protection in traffic tunnels: general aspects and results of the EUREKA project. Tunn Undergr Space Technol. 1998;13(4):377–81.
3. Hong W. The progress and controlling situation of Daegu Subway fire disaster. In: Sixth Asia-Oceania symposium on fire science and technology. Daegu: International Association for Fire Safety Science; 2004. p. 17–20.
4. Chiam BH. Numerical simulation of a metro train fire. Master Dissertation, University of Canterbury, New Zealand; 2005.
5. Dowling V, White N, Webb A, Barnett J. When a passenger train burns, how big is the fire? Invited Lecture. In: Proceedings of the 7th Asia-Oceania symposium on fire science and technology. Hong Kong: International Association for Fire Safety Science; 2007. p. 19–28.
6. Roh JS, Ryou HS, Park WH, Jang YJ. CFD simulation and assessment of life safety in a subway train fire. Tunn Undergr Space Technol. 2009;24(4):447–53.
7. White N. Fire development in passenger trains. Master Dissertation, Victoria University, Australia. 2010.
8. Kumm M. Carried Fire Load in Mass Transport Systems: A study of occurrence, allocation and fire behaviour of bags and luggage in metro and commuter trains in Stockholm. Technical Report: SiST 2010:4, Sweden: Mälardalen University Press; 2010.
9. Lönnermark A, Lindström J, Li Y. Model-scale metro car fire tests. SP report 2011:33, SP Technical Research Institute of Sweden; 2011.
10. Schebel K, Meacham BJ, Dembsey NA, Johann M, Tubbs J, Alston J. Fire growth simulation in passenger rail vehicles using a simplified flame spread model for integration with CFD analysis. J Fire Prot Eng. 2012;22(3):197–225.
11. Ingason H, Kumm M, Nilsson D, Lönnermark A, Claesson A, Li YZ et al. The METRO project, final report. Technical Report: SiST 2012:8, Sweden: Mälardalen University Press; 2012.
12. Li YZ, Ingason H, Lönnermark A. Correlations between different scales of metro carriage fire tests. In: 11th international symposium on fire safety science. Christchurch, New Zealand: International Association for Fire Safety Science; 2013.
13. Luche J, Mathis E, Rogaume T, Richard F, Guillaume E. High-density polyethylene thermal degradation and gaseous compound evolution in a cone calorimeter. Fire Saf J. 2012;54:24–35.
14. Luche J, Rogaume T, Richard F, Guillaume E. Characterization of thermal properties and analysis of combustion behavior of PMMA in a cone calorimeter. Fire Saf J. 2011;46(7):451–61.
15. An W, Jiang L, Sun J, Liew K. Correlation analysis of sample thickness, heat flux, and cone calorimetry test data of polystyrene foam. J Therm Anal Calorim. 2015;119(1):229–38.

16. Xu Q, Jin C, Griffin G, Jiang Y. Fire safety evaluation of expanded polystyrene foam by multi-scale methods. J Therm Anal Calorim. 2014;115(2):1651–60.

17. Xu Q, Jin C, Jiang Y. Analysis of the relationship between MCC and thermal analysis results in evaluating flammability of EPS foam. J Therm Anal Calorim. 2014;118:687–93.

18. Qu H, Liu C, Wu W, Chen L, Xu J. Using cone calorimeter to study thermal degradation of flexible PVC filled with zinc ferrite and Mg (OH)$_2$. J Therm Anal Calorim. 2014;115(2):1081–7.

19. Shi L, Chew MYL. Experimental study of woods under external heat flux by autoignition. J Therm Anal Calorim. 2013;111(2):1399–407.

20. Chen X, Lu S, Li C, Zhang J, Liew KM. Experimental study on ignition and combustion characteristics of typical oils. Fire Mater. 2014;38(3):409–17.

21. Song L, Zhou S, Wu J, Hu Y. Synergistic effects of lanthanum oxide on magnesium hydroxide flame-retarded ethylene propylene diene terpolymer composite. Polym Plast Technol. 2009;48(10):1088–93.

22. Du L, Xu G, Zhang Y, Qian J, Chen J. Synthesis and properties of a novel intumescent flame retardant (IFR) and its application in halogen-free flame retardant ethylene propylene diene terpolymer (EPDM). Polym Plast Technol. 2011;50(4):372–8.

23. Shen ZQ, Chen L, Lin L, Deng CL, Zhao J, Wang YZ. Synergistic effect of layered nanofillers in intumescent flame-retardant EPDM: montmorillonite versus layered double hydroxides. Ind Eng Chem Res. 2013;52(25):8454–63.

24. Yen YY, Wang HT, Guo WJ. Synergistic effect of aluminum hydroxide and nanoclay on flame retardancy and mechanical properties of EPDM composites. J Appl Polym Sci. 2013;130(3):2042–8.

25. Quintiere J. A theoretical basis for flammability properties. Fire Mater. 2006;30(3):175–214.

26. Quang Dao D, Luche J, Richard F, Rogaume T, Bourhy-Weber C, Ruban S. Determination of characteristic parameters for the thermal decomposition of epoxy resin/carbon fibre composites in cone calorimeter. Int J Hydrog Energ. 2013;38(19):8167–78.

27. Batiot B, Luche J, Rogaume T. Thermal and chemical analysis of flammability and combustibility of fir wood in cone calorimeter coupled to FTIR apparatus. Fire Mater. 2014;38(3):418–31.

28. ISO 871. Plastics: determination of ignition temperature using a hot air furnace. 3rd ed. Geneva: International Organization for Standardization (ISO); 2006.

29. ISO 1716. Reaction to fire tests for products-determination of the gross heat of combustion (calorific value). 3rd ed. Geneva: International Organization for Standardization (ISO); 2010.

30. ISO 5660. Reaction-to-fire tests-heat release, smoke production and mass loss rate-part 1: heat release rate (cone calorimeter method). 2nd ed. Geneva: International Organization for Standardization; 2002.

31. Babrauskas V. The Cone Calorimeter. In: DiNenno PJ, editor. SFPE handbook of fire protection engineering. 3rd ed. Quincy: National Fire Protection Association; 2002. p. 3.63–81.

32. Twilley WH, Babrauskas V. User's guide for the cone calorimeter. SP-745. Gaithersburg: National Institute of Standards and Technology; 1988.

33. ISO 17554. Reaction to fire-mass loss measurement. Geneva: International Organization for Standardization; 1998.

34. Babrauskas V. Ignition handbook: principles and applications to fire safety engineering, fire investigation, risk management and forensic science. 2nd ed. Issaquah: Fire Science; 2003.

35. Mouritz AP, Gibson A. Fire properties of polymer composite materials. Dordrecht: Springer; 2007.

36. Janssens M. Piloted ignition of wood: a review. Fire Mater. 1991;15(4):151–67.

37. Janssens M. Improved method of analysis for the LIFT apparatus, part I: ignition. In: Proceedings of the 2nd fire and materials conference. London, England: Interscience Communications; 1993. p. 37–46.

38. Delichatsios MA. Piloted ignition times, critical heat fluxes and mass loss rates at reduced oxygen atmospheres. Fire Saf J. 2005;40(3):197–212.

39. Janssens M, Kimble J, Murphy D. Computer tools to determine material properties for fire growth modeling from cone calorimeter data. In: 8th Proceedings of fire and materials. San Francisco, USA: Interscience Communications Limited; 2003. p. 377–87.

40. Delichatsios M, Panagiotou T, Kiley F. The use of time to ignition data for characterizing the thermal inertia and the minimum (critical) heat flux for ignition or pyrolysis. Combust Flame. 1991;84(3):323–32.

41. Janssens M. Fundamental thermophysical characteristics of wood and their role in enclosure fire growth. PhD dissertation, Ghent University, Belgium; 1991.

42. Mikkola E, Wichman IS. On the thermal ignition of combustible materials. Fire Mater. 1989;14(3):87–96.

43. Shi L, Chew MYL. Fire behaviors of polymers under autoignition conditions in a cone calorimeter. Fire Saf J. 2013;61:243–53.

44. Karlsson B, Quintiere JG. Enclosure fire dynamics. New York: CRC Press; 2000.

45. Chen R, Lu S, Zhang B, Li C, Lo S. Correlation of rate of gas temperature rise with mass loss rate in a ceiling vented compartment. Chin Sci Bull. 2014;59(33):4559–67.

46. Rhodes B, Quintiere J. Burning rate and flame heat flux for PMMA in a cone calorimeter. Fire Saf J. 1996;26(3):221–40.

47. Rhodes B. Burning rate and flame heat flux for PMMA in the cone calorimeter. NIST-GCR-95-664. Gaithersburg: National Institute of Standards and Technology; 1994.

48. Quintiere J, Rhodes B. Fire growth models for materials. NIST-GCR-94-647. Gaithersburg: National Institute of Standards and Technology; 1994.

49. Hopkins D, Quintiere JG. Material fire properties and predictions for thermoplastics. Fire Saf J. 1996;26(3):241–68.

50. Dillon S, Kim W, Quintiere JG. Determination of properties and the prediction of the energy release rate of materials in the ISO 9705 Room-corner Test. NIST-GCR-98-753. Gaithersburg: National Institute of Standards and Technology; 1998.

51. Quintiere J, Rangwala A. A theory for flame extinction based on flame temperature. Fire Mater. 2004;28(5):387–402.

52. Chen R, Lu S, Li C, Li M, Lo S. Characterization of thermal decomposition behavior of commercial flame-retardant ethylene-propylene-diene monomer (EPDM) rubber. J Therm Anal Calorim. 2015;. doi:10.1007/s10973-015-4701-2.

53. Babrauskas V, Peacock RD. Heat release rate: the single most important variable in fire hazard. Fire Saf J. 1992;18(3):255–72.

54. Thornton W. The relation of oxygen to the heat of combustion of organic compounds. Lond Edinb Dublin Philos Mag J Sci. 1917;33(194):196–203.

55. Janssens M. Measuring rate of heat release by oxygen consumption. Fire Technol. 1991;27(3):234–49.

56. Stoliarov SI, Crowley S, Lyon RE, Linteris GT. Prediction of the burning rates of non-charring polymers. Combust Flame. 2009;156(5):1068–83.